ACS EARTH AND SPACE CHEMISTRY

http://pubs.acs.org/journal/aesccq

Article

Simultaneous Insight into Dissolution and Aggregation of Metal Sulfide Nanoparticles through Single-Particle Inductively Coupled Plasma Mass Spectrometry

Muammar Mansor,* Hugo Alarcon, Jie Xu, James F. Ranville, and Manuel D. Montaño

Cite This: https://doi.org/10.1021/acsearthspacechem.1c00368

Read Online

ACCESS | Metrics & More | Article Recommendations | Supporting Information

ABSTRACT: Nanoparticles (NPs) and their colloidal aggregates are ubiquitous and play important roles in the transport and release of metals. Knowledge of their dissolution rates and aggregation behavior in solution are crucial for better prediction of their fate in biogeochemical cycling, ecotoxicity, and environmental remediation. There are however significant technical challenges to accurately obtain such information as a result of the heterogeneity and highly dynamic transformation exhibited by NPs, particularly at relatively low particle concentrations in aqueous systems. Here, we quantitatively examine the simultaneous dissolution and aggregation behavior of metal sulfide NPs using single-particle inductively coupled plasma mass spectrometry (spICP−MS). We focus on nickel sulfide (NiS), with additional data presented for copper sulfide (CuS) and cobalt sulfide (CoS). The kinetics of metal release (dissolution and disaggregation) of NiS was fastest under strongly oxidizing conditions (from 0.04 to >3 min^{-1} with H_2O_2) and were slower under near-neutral (HEPES buffer/H_2O) and acidic (1 mM HNO_3) conditions (≤0.006 min^{-1}). Metal release kinetics in HNO_3 was not faster than in H_2O or HEPES, suggesting that the solution pH has an influence over both the dissolution kinetics of individual particles and the NP aggregation states, which in combination affect metal release rates over time. Between different metal sulfides, the measured metal release rates were largely consistent with predictions based on the crystallinity, solubility products, and specific surface areas of the NPs, following an order of CoS > NiS > CuS. The spICP−MS approach described here can be easily applied to the characterization of metal release and aggregation of other NPs at low concentrations (~10^5 particles/mL) typically found in natural environments.

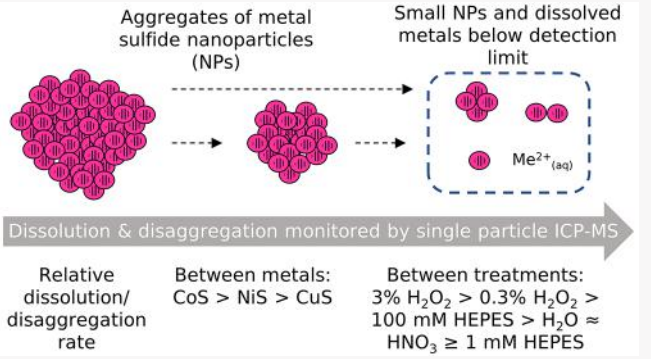

KEYWORDS: *single-particle ICP−MS, metal sulfides, nanoparticles, aggregation, dissolution*

INTRODUCTION

Nanoparticles (NPs, <100 nm) and colloidal aggregates (1−1000 nm) are ubiquitous and play important roles in the transport and release of metals.[1] For example, transition metals, such as nickel (Ni), copper (Cu), and cobalt (Co), exist as various nanoparticulate metal oxides and sulfides depending upon the redox conditions.[2,3] The kinetics of metal release from these NPs are important in evaluating their bioavailability as nutrient sources and potential toxicity as well as evaluating their long-term efficiency in remediation efforts.

The dissolution kinetics of metal-bearing NPs can be determined through several methods, with sequential filtration and transmission electron microscopy (TEM) being the most common. In sequential filtration, suspensions containing particles are filtered through various pore sizes and subsequently quantified over time, providing a measurement of the operationally defined "dissolved" (<0.45 or 0.22 μm) and particulate fraction. This technique averages within a size fraction determined by the experimenter (i.e., <3 kDa for truly dissolved and between 3 kDa and 450 nm for colloids), thus providing little insights into the dissolution mechanisms of the NPs, which form various-sized aggregates with potentially different reactivities in solution. Alternatively, time-resolved TEM has been used to provide insights into particle dissolution as a function of the size, shape, and aggregation at the nanoscale.[4−7] To link to macroscale processes, however, the changes in size of many particles need to be quantified, which is often tedious and unfeasible. Both techniques are also often applied at high initial particle concentrations (mg/L) that are not representative of inorganic particle concentrations commonly found in natural aqueous environments (μg/L).[8] Previous studies have shown that the dissolution and

Special Issue: Hochella Honorary

Received: October 29, 2021
Revised: February 1, 2022
Accepted: February 1, 2022

Table 1. Properties of the Starting Metal Sulfide NPs

NPs	size and shape of primary NPs	formula	metal mass fraction	density (g/cm^3)[b]	dried SSA (m^2/g)[c]	initial concentration[a] total (ppb)	initial concentration[a] "dissolved" (ppb)	initial concentration[a] particles/mL ($\times 10^5$)
NiS	5 ± 1 nm spheres	$Ni_{1.1}S{\cdot}1.5H_2O$	0.524	5.5	50	0.6 ± 0.3 (17)	0.4 ± 0.2 (12)	1.8 ± 0.4 (12)
CuS	<10 nm fine NPs, 30 nm nanoplates, and ~30 × 8 nm nanorods	CuS (covellite)	0.665	4.6	32	2.2 ± 0.5 (4)	0.7 ± 0.01 (2)	9.4 ± 0.1 (2)
CoS	unresolved, tend to form irregular aggregates of >50 nm	$CoS_{1.00-1.38}{\cdot}xH_2O$	0.648[d]	6.1	113	4.9 ± 1.1 (6)	0.9 ± 0.05 (3)	16.3 ± 0.8 (3)

[a]Averaged across all treatments. "Dissolved" refers to the concentrations of truly dissolved phase + particles below the spICP−-MS detection limit. Numbers in parentheses indicated the number of samples from which statistics were derived. H_2O_2-treated samples were excluded from the calculations of initial "dissolved" and particle concentrations as a result of rapid metal release before the first measurements. [b]On the basis of the values for millerite (trigonal NiS), covellite (hexagonal CuS), and jaipurite (hexagonal CoS) listed in the Materials Project Database, version 2020_09_08 (https://materialsproject.org).[32] [c]SSA = specific surface area, with a typical error of ±6%. [d]Calculated assuming stoichiometric CoS.

aggregation of NPs changed significantly as a function of the initial particle concentrations.[9,10]

Single-particle inductively coupled plasma mass spectrometry (spICP−MS) is an established nanoanalysis technique uniquely suited to fill the technical gap between sequential filtration and TEM. spICP−MS relies on the detection of pulses generated by single particles entering the plasma in a time-resolved mode.[11,12] To avoid coincidence (i.e., two particles entering the plasma at the same time), the technique is optimized for quantifying particle concentrations of ~10^6 particles/mL or lower, a number considerably more representative of environmental concentrations. spICP−MS also allows for simultaneous quantification of the particle and dissolved phases. Information can be gained on particle number concentrations (particles/mL) and their mass distribution, which can be integrated to obtain the total particle mass concentration (μg/L) or converted to particle size assuming a certain particle shape, density, and mass fraction of the measured metal. At the same time, the concentration of dissolved metals can be obtained from the background intensities that comprise the baseline. This technique has high throughput, rapidly yielding simultaneous information on the dynamics of the particle and dissolved phases. Consequently, spICP−MS has been used to quantify NP dissolution[13,14] and aggregation,[15−18] although these processes have often been studied separately. One study determined the relative dominance of particle aggregation at high initial concentrations relative to dissolution at low concentrations.[10] However, the feasibility of determining the influence of aggregation on dissolution in dilute suspensions was never demonstrated for this technique. It is important to note that the "dissolved" phase detectable in spICP−MS may also include NPs below the instrument detection limit, which corresponds to ~20−50 nm NPs for transition metals (after converting from mass to size assuming a certain shape, composition, and density; see Table S2 in ref 19). Hence, "dissolution rates" obtained from spICP−MS are better described as "metal release" rates, in which large NPs and aggregates decrease in size to a mixture of smaller, more bioavailable particles and truly dissolved metals.

Here, we describe the application of spICP−MS to constrain the metal release kinetics of several metal sulfide NPs and their aggregates at near-neutral [with 4-(2-hydroxyethyl)-1-piperazineethanesulfonic acid (HEPES) buffer or H_2O], acidic (with HNO_3), or strongly oxidizing (with H_2O_2) conditions. We focus on nickel sulfide (NiS), with additional data presented for copper sulfide (CuS) and cobalt sulfide (CoS). These metal sulfide NPs have been found as precipitates in acid mine drainages,[20] hydrothermal systems,[21] metal-contaminated soils,[22,23] and microbial cultures.[24,25] Their occurrences have furthermore been predicted on the basis of geochemical data from acidic modern soils and sediments and the ancient oceans.[26−28] Their formation is particularly favored in systems with high transition metal to iron ratios,[29−31] such as in some industrial wastewaters, mining wastes, and weathering bedrocks naturally rich in transition metals. Metal release kinetics of these metal sulfide NPs were derived and compared to the respective properties of the metal sulfides. The effects of aggregation on retarding metal release were evident, especially under acidic conditions. Our approach can be expanded for spICP−MS characterization of other NPs and their aggregates at relatively low initial concentrations (~10^5 particles/mL) that typify natural environments.

EXPERIMENTAL SECTION

Materials. NPs of NiS, CuS, and CoS were abiotically synthesized as described previously.[29−31] These NPs had been extensively characterized by TEM and X-ray diffraction (XRD) in prior studies; variations between batches were found to be minimal as long as the synthesis conditions were the same. Briefly, 0.5 mM (~60 000 ppb) dissolved metals were titrated with excess sulfide under anoxic conditions (pH 7.2−8.2). NPs formed immediately upon sulfide addition and were allowed to age for <5 days at 25 °C, before aging was halted by storage in sealed and purged serum vials with a N_2 headspace at 4 °C. Formed NiS had an average spheroidal size of 5 ± 1 nm with a chemical formula of $Ni_{1.1}S{\cdot}1.5H_2O$. The minerals were polyphasic in nature with a crystalline millerite-like core and a Ni-rich hydrated amorphous shell.[29] Formed CuS was composed of heterogeneous mixtures of covellite NPs as fine spheroidal particles, nanorods, and nanoplates, all <100 nm in size.[31] Formed CoS was XRD-amorphous and tended to form irregularly shaped aggregates of >50 nm in size. This precipitate was slightly sulfur-rich and was associated with structural water, with a poorly defined formula of $CoS_{1.00-1.38}{\cdot}xH_2O$.[30] More information on these NPs is summarized in Table 1.

Sample Preparation. Stock metal sulfide NP suspensions were rehomogenized by hand-shaking, and an aliquot (taken using N_2-flushed syringes) was then serially diluted in either H_2O or HEPES buffer at pH 7. HEPES is a zwitterionic buffer. Given that it has a pK_a of 7.5 and is thought to be inert, it is

https://doi.org/10.1021/acsearthspacechem.1c00368
ACS Earth Space Chem. XXXX, XXX, XXX−XXX

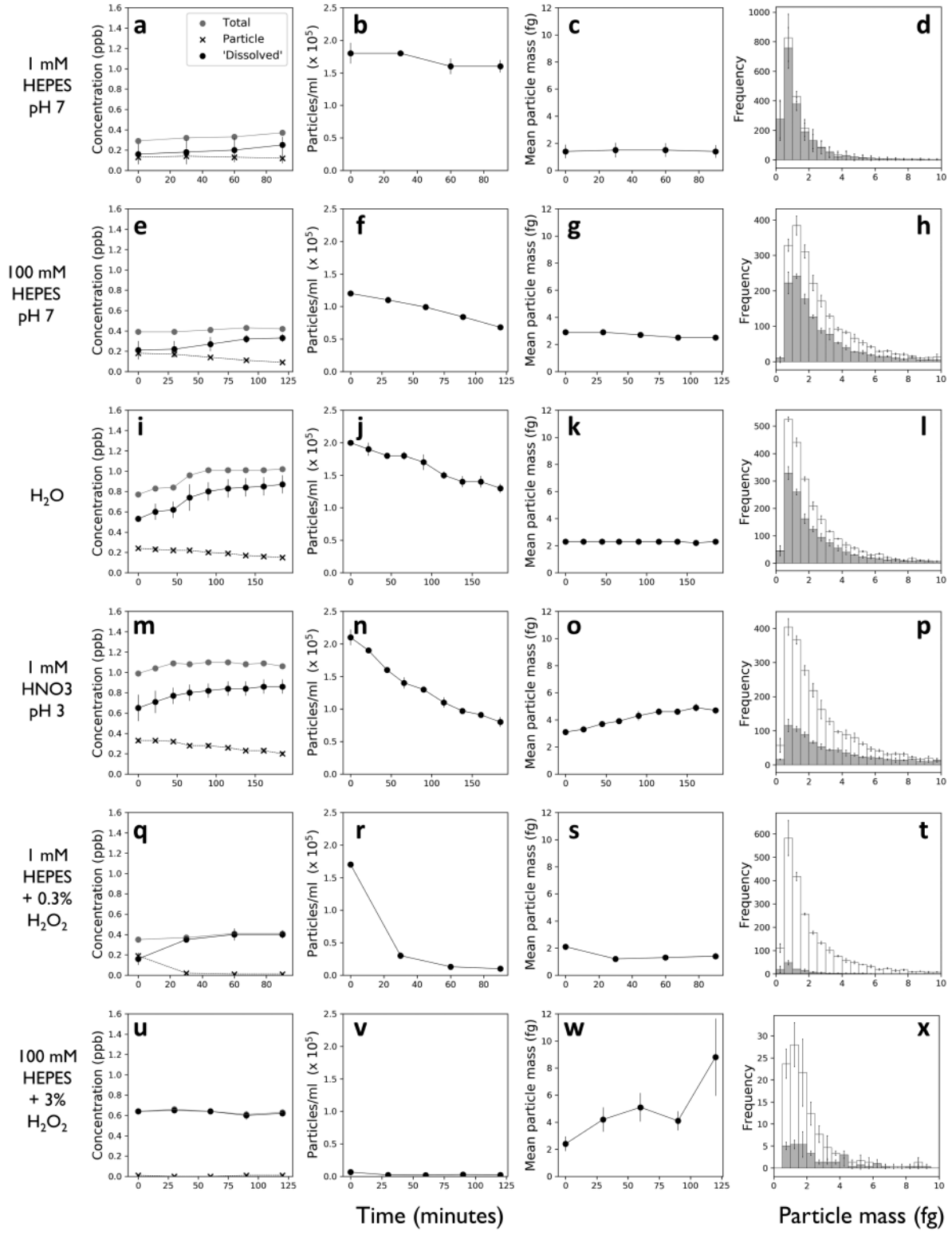

Figure 1. Summary of the spICP−MS results for NiS experiments. Results from different solution matrices are arranged in rows, from approximately the lowest (top) to highest (bottom) relative change in "dissolved" Ni. Different parameters are arranged by columns: first column, concentrations of "dissolved", particulate, and total Ni; second column, particle number concentration; third column, number-weighted mean particle mass; and fourth column, frequency histogram (with 0.5 fg bins) of particle mass at initial (white bars) and final (gray bars) time points. Note the different *x* axis for time for panels in the first three columns. Error bars represent either standard deviations (from triplicate tubes) or the data range (duplicate tubes) and are sometimes covered by the marker.

commonly used in experiments to maintain a near-neutral pH. Samples were prepared as triplicates in three separate tubes and bath-sonicated for 10 min. A small volume of concentrated reagents (16 M HNO_3 or 30% H_2O_2) was then added to the

https://doi.org/10.1021/acsearthspacechem.1c00368
ACS Earth Space Chem. XXXX, XXX, XXX−XXX

desired final concentration just before analysis. Dissolution was monitored in six different solution matrices: unbuffered H_2O, 1 mM HNO_3 (pH 3), 100 mM HEPES buffer with and without 3% H_2O_2 (pH 7), and 1 mM HEPES buffer with and without 0.3% H_2O_2 (pH 7).

spICP−MS Analysis. The dissolution of metal sulfide NPs and their aggregates in solution was monitored via spICP−MS (NexION 300D, PerkinElmer; Colorado School of Mines) on 3 separate days. Fresh dilutions of standards (0−20 ppb of Ni/Cu/Co in 2% HNO_3) and samples were prepared every day. The transport efficiency (TE) was determined every day based on the particle mass method by comparing the median intensity of 5 ppb of 100 nm gold (Au) NP standards (BBI Solutions) to dissolved Au (0−20 ppb in 2% HCl, SPEX CertiPrep).[33] Masses at ^{197}Au, ^{60}Ni, ^{59}Co, or ^{63}Cu were analyzed using a dwell time of 100 μs, radio frequency (RF) power of 1600 V, sampling depth of 3 mm, sample flow rate of 0.3 mL/min, and total data collection time of 45−60 s. Data analysis was performed via a custom Python script following the approaches of Pace et al.[33] Particle pulses were identified as those with intensities above the threshold background intensity, which was defined as the mean + 3 standard deviation of the average background. Less than 15 particles were detected in blanks, while 900−20 000 particles were detected in samples (except samples that were treated with H_2O_2, in which metal release was near complete). Hence, there was a maximum of 2% false-positive particle signals; no blank corrections were therefore applied. The total intensity of each particle pulse is summed by consecutive readings above the threshold (applying a criterion for a minimum consecutive reading of three data points), from which the mass can be determined and collected to generate a mass distribution histogram. Metal mass was converted to particle size by assuming the known mass fraction, shape, and density (Table 1). The number of particle pulses and the particle mass were summed and converted to the particle number concentration (particles/mL) and particle mass concentration (μg/L), respectively, after applying the correction for TE and flow rate. The average background intensity corresponds to the concentration of the "dissolved" phases, which also included particles smaller than the detection limit. Each sample consisted of measurements from either duplicate or triplicate tubes every 20−30 min for 90−185 min, with homogenization by inverting the tube every time just before sampling. Error bars indicate standard deviation from triplicate tubes (most samples) or the data range from duplicate tubes (for NiS and CuS samples dissolved in 1 mM HEPES with and without 0.3% H_2O_2).

Dynamic Light Scattering (DLS), XRD, and Surface Area Measurements. The particle hydrodynamic diameter was determined via DLS on the Zetasizer Nano. The same NP stock suspension and dilution procedure as described in the previous section was employed to obtain a final suspension containing 5 ppm of metal sulfides. Samples were analyzed using the default options: 173° backscatter measurement angle, automatic number of runs, run duration, positioning and attenuation selection to achieve count rates of 100−500 kilocounts per second, 3 repeat measurements, and general purpose (normal resolution) analysis model.

To obtain enough samples for surface area analysis, 100 mM solutions of dissolved metals were mixed with excess sulfide (final pH ≈ 4). Three cycles of washing with N_2-degassed water and centrifugation at 12000*g* for 15 min under anoxic conditions were performed for particle collection. For mineralogy examination with XRD, samples were dried as thin films on glass slides under a N_2−H_2 atmosphere. Individual scans were collected using a Rigaku MiniFlex II equipped with a Cu Kα source from 10 to 60° 2θ with a step size of 0.05° and a scan speed of 0.25°/min, totaling a collection time of ∼3.3 h per sample (Figure S1 of the Supporting Information). Dried samples were also shipped in sealed serum vials to the NanoEarth National Center at Virginia Tech. On site, the samples were unsealed and degassed at 100 °C overnight under high vacuum. Surface areas were then determined via N_2 adsorption data by the seven-point Brunauer−Emmett−Teller (BET) method. No unexpected or unusually high safety hazards were encountered throughout the methods outlined here.

RESULTS AND DISCUSSION

Simultaneous Insight into Particle and "Dissolved" Metal Dynamics during Dissolution. The release of metals (dissolution + disaggregation to small NPs below the detection limit) from NiS was monitored for up to 185 min in six different solution matrices: unbuffered H_2O, 1 mM HNO_3 (pH 3), 100 mM HEPES buffer with and without 3% H_2O_2 (pH 7), and 1 mM HEPES buffer with and without 0.3% H_2O_2 (pH 7). Over 3 separate measurement days, the TE varied over a relatively small range from 3.7 to 5.9%. The initial total Ni concentrations averaged 0.6 ± 0.3 ppb across all treatments (Table 1). The initial "dissolved" Ni concentrations varied from around 0.2 to 0.6 ppb and made up 13−99% of the total Ni concentrations. Considering the solubility product of NiS NPs[34] and millimolar levels of excess sulfide in the undiluted stock NP suspension,[29] the concentration of truly dissolved Ni in the diluted suspensions used for the dissolution experiments should be well below the parts per billion (ppb) level. Therefore, the detectable levels of "dissolved" Ni from spICP−MS likely reflected prior dissolution during sample preparation and/or the presence of particles below the detection limit. The particle detection limit was 0.26−0.33 fg (equivalent spherical NiS size = 45−49 nm), indicating that only aggregates composed of >700 primary NiS NPs (mass/NP ≈ 4×10^{-4} fg) were detectable as particles. For NiS treated with 3% H_2O_2, "dissolved" Ni values were consistently high from the beginning and nearly equal to the total Ni concentrations, while particle detection was constantly low, suggesting that extensive metal release had taken place even before the first sampling point. Excluding this experiment, the initial particle number concentration averaged 1.8 ± 0.4 × 10^5 particles/mL across all treatments (Table 1).

Figure 1 summarizes the obtained time evolution data across all dissolution experiments. The plots are arranged from approximately the lowest (top) to highest (bottom) relative change in "dissolved" Ni. The process of metal release is best illustrated by first considering the case of NiS treated with 1 mM HNO_3 (fourth row) as an example. Following HNO_3 addition, the "dissolved" Ni concentration increased with time with a concurrent decrease in both particle mass and number concentrations (panels m and n of Figure 1). Metal release in this treatment was also reflected in the changes in particle mass distribution over time, in which there was a decrease in the particle number in nearly all histogram bins (Figure 1p). Metal release from NiS in other solution matrices yielded similar trends, albeit to different degrees depending upon the extent of dissolution and/or disaggregation. For example, metal release

https://doi.org/10.1021/acsearthspacechem.1c00368
ACS Earth Space Chem. XXXX, XXX, XXX−XXX

Table 2. Derived Metal Release Kinetics from the Experiments

	first-order rate constant, k_{m1} (min^{-1})			second-order rate constant, k_{m2} (L μg^{-1} min^{-1})		
solution matrix	NiS[a]	CuS	CoS	NiS[a]	CuS	CoS
H_2O	0.003			0.014		
	(0.977)			(0.963)		
1 mM HNO_3	0.003			0.011		
	(0.948)			(0.922)		
100 mM HEPES	0.006			0.047		
	(0.973)			(0.945)		
100 mM HEPES + 3% H_2O_2	>3[b]			>119[b]		
1 mM HEPES	0.001	NA[c]	0.002	0.011	NA[c]	0.0006
	(0.558)		(0.558)	(0.566)		(0.577)
1 mM HEPES + 0.3% H_2O_2	0.036[d]	0.013	>4[b]	1.604[d]	0.037	>18[b]
	(0.837)	(0.593)		(0.983)	(0.588)	

[a]For NiS, surface-area-normalized rate constants (k_{SA}) can be derived assuming a geometric surface area A of 218 m^2/g. The k_{SA1} values ($\mu g\ m^{-2}\ min^{-1}$) for first-order rate laws are identical to k_{m1} values. The k_{SA2} values (L $\mu g\ m^{-4}\ min^{-1}$) for second-order rate laws are equal to $k_{m2} \times 1/A$. [b]Minimum estimates as a result of rapid metal release even before the first sampling point, assuming complete metal release within 1 min. [c]Not available; fitting gave negative values as a result of low extents of metal release. [d]Significantly better fit with the second-order rate law. For all other samples, both the first- and second-order rate laws had similar R^2 values. R^2 values are given in parentheses under each sample.

was minimal for NiS in HEPES buffers (panels a−h of Figure 1), while metal release was quite rapid following treatment with H_2O_2 (panels q−x of Figure 1).

Metal release from NiS was accompanied by different trends in the mean particle mass depending upon the treatment. For NiS treated with 1 mM HNO_3, the mean particle mass increased from 3.08 ± 0.04 to 4.69 ± 0.05 fg (Figure 1o), which corresponded to an increase in the mean equivalent spherical size from 95 to 107 nm. This trend was also evident for NiS treated with 100 mM HEPES + 3% H_2O_2 (Figure 1w), although the number of particle pulses counted was statistically not significant (<40) after the initial time point for this sample. In contrast, other treatments resulted in little changes to the mean particle mass over time.

To compare metal release kinetics across treatments, rate constants (k) were derived from the time evolution of the particle mass concentration following either first- or second-order rate laws, where R_m is the metal release rate ($\mu g\ L^{-1}\ s^{-1}$) and P is the particle metal mass concentration (Ni, Cu, or Co).

$$\text{first order:} \quad R_{m1} = k_{m1}(P_t) \tag{1}$$

$$\text{second order:} \quad R_{m2} = k_{m2}(P_t)^2 \tag{2}$$

Integrating and rearranging the equations allow for solving k as the slope of $-\ln(P_t)$ or $1/(P_t)$ versus time t.

$$\text{first order:} \quad -\ln(P_t) = kt\ \ln(P_0) \tag{3}$$

$$\text{second order:} \quad \frac{1}{P_t} = k_p t + \frac{1}{P_0} \tag{4}$$

For particles, it is a common approach to normalize dissolution rates with the total particle surface area that comes into contact with solution.[35] To obtain the total surface area, the particle mass concentration can be multiplied with the surface area per mass of NiS NPs (A), assuming a geometric surface area of 218 m^2/g.

From these analyses, both the first- and second-order rate laws were found to fit the data equally well for most samples (Table 2 and panels a and b of Figure S2 of the Supporting Information). The R^2 values were larger than 0.8, except for NiS treated with 1 mM HEPES, in which metal release was minimal. In only one case (NiS treated with 1 mM HEPES + 0.3% H_2O_2) was better fitting obtained with the second-order rate law (R^2 = 0.983) versus the first-order rate law (R^2 = 0.837). While NP dissolutions are generally best explained with first-order kinetics,[35] second-order rate laws have been reported for the dissolution of silver NPs and explained in terms of slower late-stage kinetics that was influenced by significant aggregation or proximity to the solubility limit of metal ions.[36] For polyphasic NiS NPs, such as in this study, slower late-stage metal release kinetics may also be explained by a diminished rate after the amorphous shell was eroded, exposing the more crystalline and likely recalcitrant millerite core. Calculations indicate that the mass of Ni in the shell should constitute 64−99% of the total Ni depending upon the assumed NP size, core diameter, and density (Table S1 of the Supporting Information). In our experiments, 37 to over 90% of Ni was loss to the "dissolved" phase. The data and rate law are therefore consistent with loss of Ni primarily from the shell layer, but it does not rule out contribution of particle disaggregation to the measured "dissolved" phase.

The trends in metal release kinetics were the same irrespective of the rate laws used and followed the order (from fastest to slowest): 100 mM HEPES + 3% H_2O_2 > 1 mM HEPES + 0.3% H_2O_2 > 100 mM HEPES > $H_2O \approx HNO_3 \geq$ 1 mM HEPES (Table 2). Thus, metal release was rapid under strongly oxidizing conditions, while metal release was slower in HEPES buffer, H_2O, and under mildly acidic (pH 3) conditions. It was surprising that the metal release from NiS was relatively slow in HNO_3, and this will be discussed further in the next section. Surprisingly, metal release also proceeded faster at pH 7 in 100 mM HEPES than in 1 mM HEPES and H_2O (measured pH 4.4, but this value was uncertain given the low ionic strength of the sample and was likely higher given buffering by atmospheric CO_2 and residual sulfide). We considered if this was caused by solution matrix effects. A previous study found that dissolved carbon in the solution matrix contributed to overestimation of Ni concentrations.[37] A solution of 1 mM HEPES corresponds to 0.096% carbon, while a solution of 100 mM HEPES corresponds to 0.96% carbon. On the basis of linear extrapolation from Narukawa et al.,[37] we estimate negligible matrix effects for 1 mM HEPES and a potential Ni overestimation by 1.4 times in 100 mM HEPES. Correcting for this potential matrix effect however made little

https://doi.org/10.1021/acsearthspacechem.1c00368
ACS Earth Space Chem. XXXX, XXX, XXX−XXX

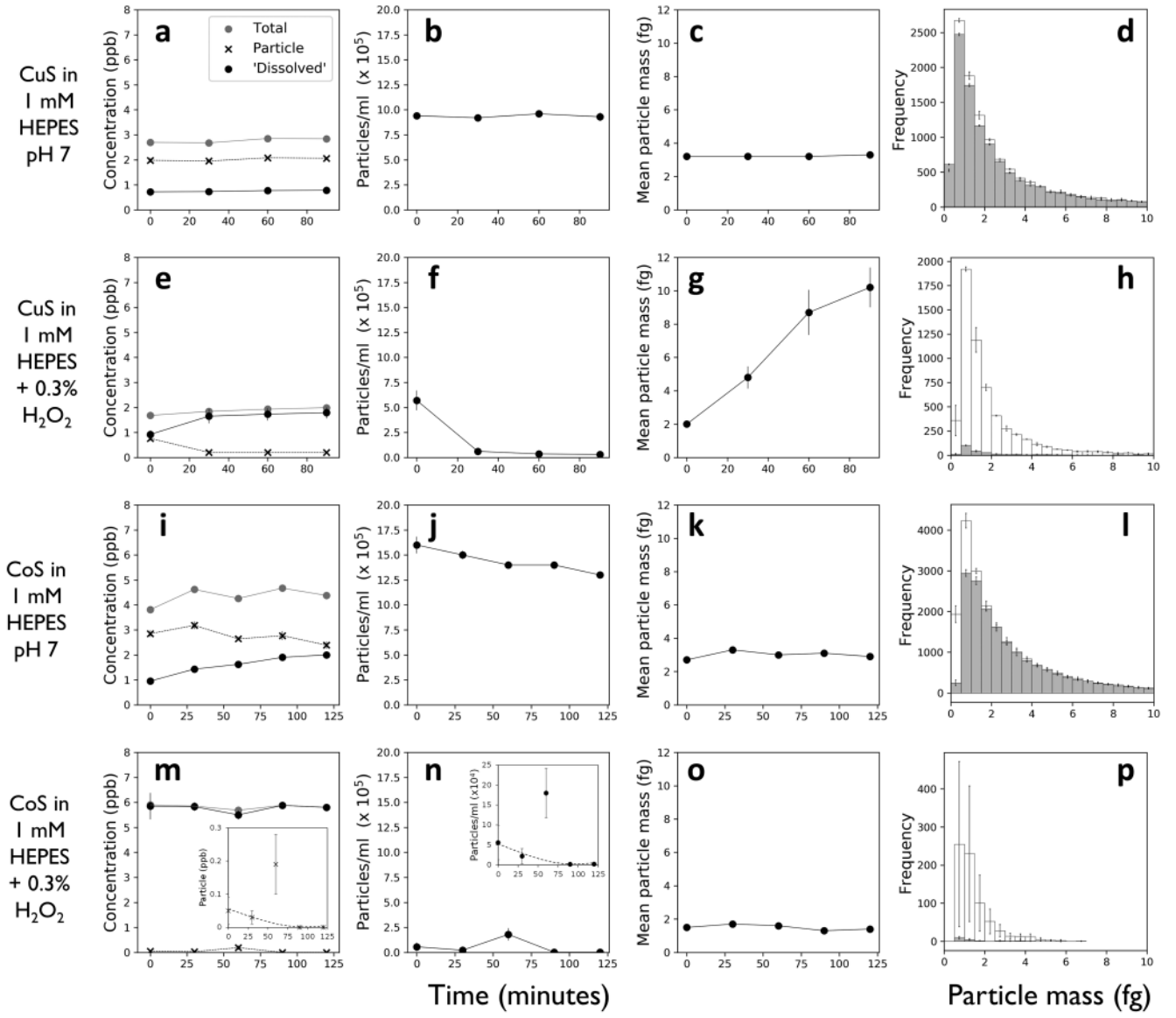

Figure 2. Summary of the spICP−MS results for CuS and CoS dissolution experiments. Different parameters are arranged by columns: column 1, concentrations of "dissolved", particulate, and total metal; column 2, particle number concentration; column 3, number-weighted mean particle mass; and column 4, frequency histogram (with 0.5 fg bins) of particle mass at initial (white bars) and final (gray bars) time points. In panels m and n, insets are provided to highlight the small change in particle mass and number concentrations.

changes to the derived rate constants listed for treatments with 100 mM HEPES, as listed in Table 2 (<0.001 min^{-1} and <0.005 L μg^{-1} min^{-1} for first- and second-order rate constants, respectively).

Why a higher concentration of HEPES contributed to faster metal release of NiS is unclear. HEPES is not known to form complexes with dissolved Ni^{2+},[38,39] which would have increased solubility and, therefore, may contribute to faster dissolution. Some buffers are known to affect surface chemistry[40] and, hence, aggregation.[41] Indeed, the mean particle mass of NiS in 100 mM HEPES is larger than that in 1 mM HEPES (compare panels g and c of Figure 1). However, this would have retarded metal release rather than accelerating it. Free radicals that could accelerate oxidative reactions have been known to be generated by HEPES in the presence of Fe or Au(III) but not in the presence of Ni.[42,43] Additionally, it was suggested that the sulfonic acid group of HEPES can act as an oxidant and be reduced to sulfide in the process.[44−46] If this reaction occurred, the reductant could either be solid-bound Ni(II) or sulfide in NiS NPs, of which either is speculative at the moment. Another possibility is that the sulfonic acid group of HEPES can react with and remove the hydroxide-rich shell layer of polyphasic NiS, similar to how sulfate is known to remove the Fe−oxyhydroxide passivation layer on the surface of zerovalent iron.[44]

In addition, we monitored the metal release from CuS and CoS in 1 mM HEPES with and without 0.3% H_2O_2 (Figure 2). We aimed for initial total metal concentrations of ∼1 ppb to be directly comparable to NiS, but the measured averaged concentrations were slightly higher for CuS (2.2 ± 0.5 ppb of Cu) and CoS (4.9 ± 1.1 ppb of Co) across all treatments (Table 1). The variation in initial concentrations between metal sulfides was likely due to uncertainties during sampling and dilution of heterogeneous aggregates from the stock

https://doi.org/10.1021/acsearthspacechem.1c00368
ACS Earth Space Chem. XXXX, XXX, XXX−XXX

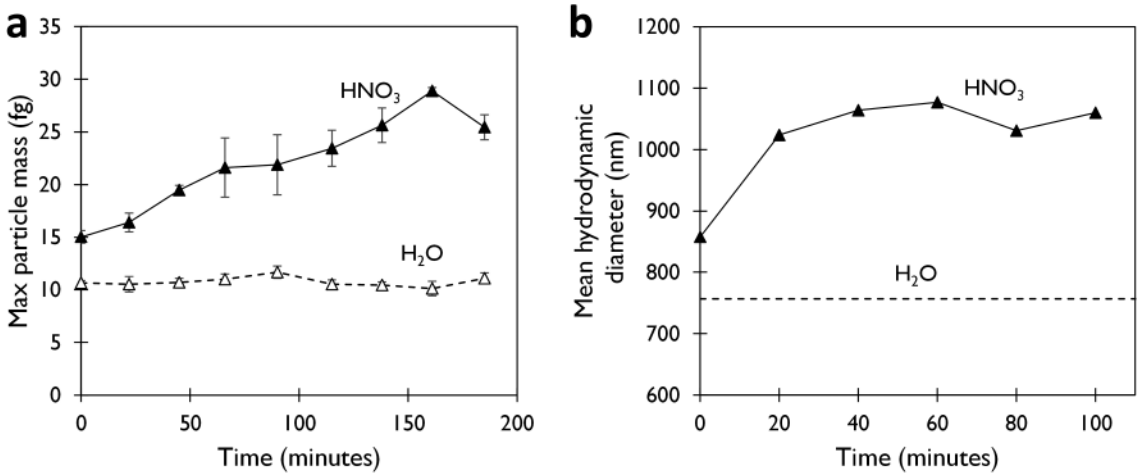

Figure 3. Changes in the particle size over time for NiS in H_2O and 1 mM HNO_3: (a) time evolution of the maximum particle mass as determined by spICP−MS and (b) time evolution of the mean hydrodynamic diameter of 5 ppm of NiS in 1 mM HNO_3. The size increased over time relative to that in H_2O (dashed line), indicative of aggregation.

suspensions. Initial "dissolved" Cu and Co concentrations were <1 ppb, indicating that the majority of the mass was contributed by NP aggregates, with masses higher than the detection limit of 0.28 fg of Cu (equivalent spherical CuS size of 49 nm) or 0.21 fg of Co (equivalent spherical CoS size of 41 nm). This was reflected in the high initial particle concentrations (excluding those with H_2O_2 addition) of 9.4 ± 0.1 × 10^5 particles/mL for CuS and 16.3 ± 0.8 × 10^5 particles/mL for CoS. Similar to NiS treated with 100 mM HEPES + 3% H_2O_2, CoS treated with 1 mM HEPES + 0.3% H_2O_2 showed a trend of consistently high "dissolved" metal and low particle concentrations from the first sampling point, indicating that rapid metal release took place (panels m−p of Figure 2). Slower release of metals was observable throughout the measurement period for this sample (insets in panels m and n of Figure 2). There were anomalous values detected at time point 60 min with large error bars between replicates. We were unable to explain their occurrences, and these anomalous values were no longer detectable at later time points.

In comparison between metal sulfides, the metal release kinetics followed the order (from fastest to slowest): CoS ≈ NiS > CuS in 1 mM HEPES and CoS > NiS > CuS with the addition of 0.3% H_2O_2 (Table 2 and Figure S2c of the Supporting Information). This trend was consistent with the respective solubility product constant of the metal sulfides (from most to least soluble): CoS (log K_{sp} = 1.2) > NiS (log K_{sp} = −2.7) > CuS (log K_{sp} = −15.8).[30,34,47,48] The slow metal release from CuS was consistent with its high stability under oxic conditions.[49−51] Additionally, the trend was also consistent with the relative crystallinity and specific surface areas (SSA) between the metal sulfides: CoS (113 m^2/g, XRD amorphous) > NiS (50 m^2/g, polyphasic) > CuS (32 m^2/g, crystalline) (Table 1). The measured SSA values were not used to derive surface-area-normalized rates because (1) these samples were not identical to the samples used for spICP−MS and (2) the SSA values measured for dried, aggregated samples via BET were likely much lower than those for NPs in suspension. The use of geometric surface areas for CoS and CuS were also not possible given their poorly constrained and heterogeneous nature, respectively. Nonetheless, the agreement of our kinetics data with solubility product constant, SSA, and crystallinity results showed that spICP−MS is an accurate and rapid technique for quantifying the metal release rates of metal-bearing NPs and their colloidal aggregates.

Effects of Aggregation on Metal Release. In the previous section, it was shown that the metal release rate constants for NiS in 1 mM HNO_3 are quite similar to those in H_2O (Table 2). This was surprising given that Ni (and other transition metals) is many times more soluble under acidic conditions.[34] An inverted trend in which Ni solubility increased with pH was observed previously but only at moderate to highly alkaline values (pH from 8 to >11) in which aqueous polysulfide complexes were estimated to be dominant;[52] this mechanism is likely not relevant to our system. At first glance, the metal release rate constants appeared to be inconsistent with the larger relative decrease of the particle number concentration and particle mass distribution of NiS in HNO_3 compared to H_2O (Figure 1; compare the third and fourth rows). These observations are best understood in terms of the primary factors controlling the metal release rate, particle number concentration, and particle mass distribution separately. A previous modeling study has shown that the particle mass concentration is only sensitive to dissolution, while the particle number concentration and mass distribution are also sensitive to aggregation.[53] Therefore, we hypothesize that more extensive particle aggregation had occurred in 1 mM HNO_3, which affected the observed particle dynamics and retarded metal release from NiS.

To test our hypothesis, the time evolutions of particle mass distribution for NiS in H_2O and HNO_3 are compared side by side (Figure 3a and Figure S3 of the Supporting Information). In H_2O, the maximum particle mass was consistently <15 fg over the duration of the experiment. In contrast, the maximum particle mass in HNO_3 continuously increased over time from 15 to ∼25 fg, indicative of the formation of larger aggregates. This was also reflected in the continuous increase in the mean particle mass for NiS in HNO_3 (Figure 1o), which was not evident for NiS in H_2O. The increase in the mean particle mass cannot be explained by a higher particle detection limit as a result of a higher "dissolved" background. Higher particle detection limits were indeed observed over time but only by as much as 0.01 fg. Over the same time period, the minimum particle mass remained comparable and even decreased slightly, signifying little effects of changes in detection limits

https://doi.org/10.1021/acsearthspacechem.1c00368
ACS Earth Space Chem. XXXX, XXX, XXX−XXX

over this small range to the overall particle population (Figure S4 of the Supporting Information). In Figure 3a, we have plotted the maximum particle mass parameter because it is largely independent of the particle detection limit, and plotting this parameter allows for unambiguous observation for the increase in aggregation at lower pH.

The observation of more extensive aggregation at lower pH is consistent with surface charge consideration; the point of zero charge of NiS NPs is not known but is estimated to be in the acidic pH range by comparison to other sulfides.[54,55] Support for our hypothesis was also corroborated through measurements of the hydrodynamic diameter by DLS. Measurements were performed at 5 ppm, ∼5000× higher than for spICP−MS analysis, as a result of the lower sensitivity of DLS. The results nonetheless showed that HNO_3 addition led to the formation of larger NiS aggregates compared to those in H_2O (Figure 3b). The polydispersity index was between 0.3 and 0.4 for all samples, which indicates moderately polydisperse suspensions.[56] Thus, aggregation of NiS NPs was favored under acidic conditions, and we hypothesize that this led to lower metal release rates than expected.

Our conclusion is consistent with studies on other metal sulfide NPs. Aggregation was found to retard the dissolution of galena (PbS), attributed to the slower diffusion rate of protons in restricted pore spaces within aggregates.[4,5] The aggregation of mackinawite (FeS) at pH 4 was also observed to limit isotopic exchange with aqueous Fe^{2+} compared to in neutral pH.[57] In general, aggregation leads to a decrease in the total reactive surface areas of particles.

Overall, our research has highlighted the power and versatility of spICP−MS. A significant portion of metal sulfide NPs was found to exist as colloidal aggregates even at relatively low concentrations that are applicable to many natural settings. Metal release kinetics was obtained from these NP aggregates, enabling evaluation of the role of NP aggregation and dissolution on metal biogeochemistry, toxicity, and sequestration efficiency. Minimal sample preparation (i.e., serial dilution) was needed for analyses. Simultaneous insight into metal release and particle behaviors was obtained; the observation of aggregation was invaluable to explain the slower than expected metal release from NPs under acidic conditions. This information would not have been gained through any other single technique in isolation.

The approaches that we outlined in this study can be applied to a plethora of metal NPs and their colloidal aggregates under many environmental conditions of interest. For example, we envision a direct application of spICP−MS in remediation to determine the fate of toxic metal contaminants being sequestered as metal sulfide NPs in aquifers and groundwaters.

■ ASSOCIATED CONTENT

Supporting Information

The Supporting Information is available free of charge at https://pubs.acs.org/doi/10.1021/acsearthspacechem.1c00368.

XRD patterns of NPs synthesized at acidic pH (Figure S1), rate-law-fitting plots for metal release kinetics (Figure S2), time evolution of particle mass distribution in histograms (Figure S3), time evolution of the particle detection limit and minimum particle mass (Figure S4), and calculation of Ni in the outer shell of polyphasic NiS (Table S1) (PDF)

■ AUTHOR INFORMATION

Corresponding Author

Muammar Mansor − *Department of Geological Sciences, The University of Texas at El Paso, El Paso, Texas 79968, United States; Geomicrobiology, Center for Applied Geosciences, University of Tuebingen, 72076 Tuebingen, Germany;* Present Address: Muammar Mansor: Geomicrobiology, Center for Applied Geosciences, University of Tuebingen, 72076 Tuebingen, Germany; orcid.org/0000-0001-7830-650X; Email: muammar.muammar-bin-mansor@uni-tuebingen.de

Authors

Hugo Alarcon − *Department of Geological Sciences, The University of Texas at El Paso, El Paso, Texas 79968, United States*

Jie Xu − *Department of Geological Sciences, The University of Texas at El Paso, El Paso, Texas 79968, United States*

James F. Ranville − *Department of Chemistry, Colorado School of Mines, Golden, Colorado 80401, United States*

Manuel D. Montaño − *Department of Environmental Sciences, Western Washington University, Bellingham, Washington 98225, United States*

Complete contact information is available at: https://pubs.acs.org/10.1021/acsearthspacechem.1c00368

Author Contributions

James F. Ranville came up with the original idea and further expanded it through several discussions with Muammar Mansor, Manuel D. Montaño, and Jie Xu. Muammar Mansor and Manuel D. Montaño performed the work. Hugo Alarcon prepared some samples and performed XRD and BET measurements. Muammar Mansor prepared the manuscript draft, and all authors contributed to manuscript revisions.

Funding

This study was funded by Grant DOE-BES DE-FG02-06ER15786 awarded by the United States Department of Energy to Jie Xu, Michael F. Hochella, and Mitsu Murayama and also by the startup package awarded to Jie Xu by The University of Texas at El Paso.

Notes

The authors declare no competing financial interest.

■ ACKNOWLEDGMENTS

The authors thank Dr. Saurav Kumar for building the original Python framework for data analysis and Weinan Leng for performing the BET analysis. This work used shared facilities at the Virginia Tech National Center for Earth and Environmental Nanotechnology Infrastructure (NanoEarth), a member of the National Nanotechnology Coordinated Infrastructure (NNCI) network, supported by the National Science Foundation (NSF) (ECCS 1542100). NanoEarth is housed at Virginia Tech's Institute for Critical Technology and Applied Sciences (ICTAS).

■ REFERENCES

(1) Hochella, M. F.; Mogk, D. W.; Ranville, J.; Allen, I. C.; Luther, G. W.; Marr, L. C.; McGrail, B. P.; Murayama, M.; Qafoku, N. P.; Rosso, K. M.; Sahai, N.; Schroeder, P. A.; Vikesland, P.; Westerhoff,

P.; Yang, Y. Natural, Incidental, and Engineered Nanomaterials and Their Impacts on the Earth System. *Science* **2019**, *363* (6434), eaau8299.
(2) Ubaid, K. A.; Zhang, X.; Sharma, V. K.; Li, L. Fate and Risk of Metal Sulfide Nanoparticles in the Environment. *Environ. Chem. Lett.* **2020**, *18* (1), 97−111.
(3) Amde, M.; Liu, J. F.; Tan, Z. Q.; Bekana, D. Transformation and Bioavailability of Metal Oxide Nanoparticles in Aquatic and Terrestrial Environments. A Review. *Environ. Pollut.* **2017**, *230*, 250−267.
(4) Liu, J.; Aruguete, D. M.; Jinschek, J. R.; Donald Rimstidt, J.; Hochella, M. F. The Non-Oxidative Dissolution of Galena Nanocrystals: Insights into Mineral Dissolution Rates as a Function of Grain Size, Shape, and Aggregation State. *Geochim. Cosmochim. Acta* **2008**, *72* (24), 5984−5996.
(5) Liu, J.; Aruguete, D. M.; Murayama, M.; Hochella, M. F., Jr. Influence of Size and Aggregation on the Reactivity of an Environmentally and Industrially Relevant Nanomaterial (PbS). *Environ. Sci. Technol.* **2009**, *43*, 8178−8183.
(6) Eskelsen, J. R.; Xu, J.; Chiu, M.; Moon, J. W.; Wilkins, B.; Graham, D. E.; Gu, B.; Pierce, E. M. Influence of Structural Defects on Biomineralized ZnS Nanoparticle Dissolution: An in-Situ Electron Microscopy Study. *Environ. Sci. Technol.* **2018**, *52* (3), 1139−1149.
(7) Echigo, T.; Aruguete, D. M.; Murayama, M.; Hochella, M. F. Influence of Size, Morphology, Surface Structure, and Aggregation State on Reductive Dissolution of Hematite Nanoparticles with Ascorbic Acid. *Geochim. Cosmochim. Acta* **2012**, *90*, 149−162.
(8) Westerhoff, P.; Atkinson, A.; Fortner, J.; Wong, M. S.; Zimmerman, J.; Gardea-Torresdey, J.; Ranville, J.; Herckes, P. Low Risk Posed by Engineered and Incidental Nanoparticles in Drinking Water. *Nat. Nanotechnol.* **2018**, *13* (8), 661−669.
(9) Hadioui, M.; Leclerc, S.; Wilkinson, K. J. Multimethod Quantification of Ag^+ Release from Nanosilver. *Talanta* **2013**, *105*, 15−19.
(10) Merrifield, R. C.; Stephan, C.; Lead, J. Determining the Concentration Dependent Transformations of Ag Nanoparticles in Complex Media: Using SP-ICP-MS and Au@Ag Core-Shell Nanoparticles as Tracers. *Environ. Sci. Technol.* **2017**, *51* (6), 3206−3213.
(11) Montaño, M. D.; Olesik, J. W.; Barber, A. G.; Challis, K.; Ranville, J. F. Single Particle ICP-MS: Advances toward Routine Analysis of Nanomaterials. *Anal. Bioanal. Chem.* **2016**, *408* (19), 5053−5074.
(12) Mansor, M.; Drabesch, S.; Bayer, T.; Van Le, A.; Chauhan, A.; Schmidtmann, J.; Peiffer, S.; Kappler, A. Application of Single-Particle ICP-MS to Determine the Mass Distribution and Number Concentrations of Environmental Nanoparticles and Colloids. *Environ. Sci. Technol. Lett.* **2021**, *8* (7), 589−595.
(13) Mitrano, D. M.; Ranville, J. F.; Bednar, A.; Kazor, K.; Hering, A. S.; Higgins, C. P. Tracking Dissolution of Silver Nanoparticles at Environmentally Relevant Concentrations in Laboratory, Natural, and Processed Waters Using Single Particle ICP-MS (SpICP-MS). *Environ. Sci. Nano* **2014**, *1* (3), 248−259.
(14) Azodi, M.; Sultan, Y.; Ghoshal, S. Dissolution Behavior of Silver Nanoparticles and Formation of Secondary Silver Nanoparticles in Municipal Wastewater by Single-Particle ICP-MS. *Environ. Sci. Technol.* **2016**, *50* (24), 13318−13327.
(15) Kim, H. A.; Lee, B. T.; Na, S. Y.; Kim, K. W.; Ranville, J. F.; Kim, S. O.; Jo, E.; Eom, I. C. Characterization of Silver Nanoparticle Aggregates Using Single Particle-Inductively Coupled Plasma-Mass Spectrometry (SpICP-MS). *Chemosphere* **2017**, *171*, 468−475.
(16) Rand, L. N.; Ranville, J. F. Characteristics and Stability of Incidental Iron Oxide Nanoparticles during Remediation of a Mining-Impacted Stream. *Environ. Sci. Technol.* **2019**, *53* (19), 11214−11222.
(17) Nwoko, K. C.; Raab, A.; Cheyne, L.; Dawson, D.; Krupp, E.; Feldmann, J. Matrix-Dependent Size Modifications of Iron Oxide Nanoparticles (Ferumoxytol) Spiked into Rat Blood Cells and Plasma: Characterisation with TEM, AF4-UV-MALS-ICP-MS/MS and SpICP-MS. *J. Chromatogr. B: Anal. Technol. Biomed. Life Sci.* **2019**, *1124* (June), 356−365.
(18) António, D. C.; Cascio, C.; Jakšić; Jurašin, D.; Lyons, D. M.; Nogueira, A. J. A.; Rossi, F.; Calzolai, L. Assessing Silver Nanoparticles Behaviour in Artificial Seawater by Mean of AF4 and SpICP-MS. *Mar. Environ. Res.* **2015**, *111*, 162−169.
(19) Lee, S.; Bi, X.; Reed, R. B.; Ranville, J. F.; Herckes, P.; Westerhoff, P. Nanoparticle Size Detection Limits by Single Particle ICP-MS for 40 Elements. *Environ. Sci. Technol.* **2014**, *48* (17), 10291−10300.
(20) Hochella, M. F.; Moore, J. N.; Putnis, C. V.; Putnis, A.; Kasama, T.; Eberl, D. D. Direct Observation of Heavy Metal-Mineral Association from the Clark Fork River Superfund Complex: Implications for Metal Transport and Bioavailability. *Geochim. Cosmochim. Acta* **2005**, *69* (7), 1651−1663.
(21) Gartman, A.; Findlay, A. J.; Luther, G. W. Nanoparticulate Pyrite and Other Nanoparticles Are a Widespread Component of Hydrothermal Vent Black Smoker Emissions. *Chem. Geol.* **2014**, *366*, 32−41.
(22) Mantha, H.; Schindler, M.; Hochella, M. F. Occurrence and Formation of Incidental Metallic Cu and CuS Nanoparticles in Organic-Rich Contaminated Surface Soils in Timmins, Ontario. *Environ. Sci. Nano* **2019**, *6* (1), 163−179.
(23) Hofacker, A. F.; Voegelin, A.; Kaegi, R.; Weber, F. A.; Kretzschmar, R. Temperature-Dependent Formation of Metallic Copper and Metal Sulfide Nanoparticles during Flooding of a Contaminated Soil. *Geochim. Cosmochim. Acta* **2013**, *103*, 316−332.
(24) Ferris, F. G.; Fyfe, W. S.; Beveridge, T. J. Bacteria as Nucleation Sites for Authigenic Minerals in a Metal-Contaminated Lake Sediment. *Chem. Geol.* **1987**, *63*, 225−232.
(25) Park, Y.; Faivre, D. Diversity of Microbial Metal Sulfide Biomineralization. *ChemPlusChem* **2022**, *87* (1), e202100457.
(26) Moore, E. K.; Hao, J.; Prabhu, A.; Zhong, H.; Jelen, B. I.; Meyer, M.; Hazen, R. M.; Falkowski, P. G. Geological and Chemical Factors That Impacted the Biological Utilization of Cobalt in the Archean Eon. *J. Geophys. Res.: Biogeosci.* **2018**, *123* (3), 743−759.
(27) Huerta-Diaz, M. A.; Tessier, A.; Carignan, R. Geochemistry of Trace Metals Associated with Reduced Sulfur in Freshwater Sediments. *Appl. Geochem.* **1998**, *13* (2), 213−233.
(28) Frohne, T.; Rinklebe, J.; Diaz-Bone, R. A.; Du Laing, G. Controlled Variation of Redox Conditions in a Floodplain Soil: Impact on Metal Mobilization and Biomethylation of Arsenic and Antimony. *Geoderma* **2011**, *160* (3−4), 414−424.
(29) Mansor, M.; Winkler, C.; Hochella, M. F., Jr.; Xu, J. Nanoparticulate Nickel-Hosting Phases in Sulfidic Environments: Effects of Ferrous Iron and Bacterial Presence on Mineral Formation Mechanism and Solid-Phase Nickel Distribution. *Front. Earth Sci.* **2019**, *7*, 151.
(30) Mansor, M.; Cantando, E.; Wang, Y.; Hernandez-Viezcas, J. A.; Gardea-Torresdey, J. L.; Hochella, M. F., Jr.; Xu, J. Insights into the Biogeochemical Cycling of Cobalt: Precipitation and Transformation of Cobalt Sulfide Nanoparticles under Low-Temperature Aqueous Conditions. *Environ. Sci. Technol.* **2020**, *54* (9), 5598−5607.
(31) Mansor, M.; Berti, D.; Hochella, M. F., Jr.; Murayama, M.; Xu, J. Phase, Morphology, Elemental Composition and Formation Mechanisms of Biogenic and Abiogenic Fe-Cu-Sulfide Nanoparticles: A Comparative Study on Their Occurrences under Anoxic Conditions. *Am. Mineral.* **2019**, *104* (5), 703−717.
(32) Jain, A.; Ong, S. P.; Hautier, G.; Chen, W.; Richards, W. D.; Dacek, S.; Cholia, S.; Gunter, D.; Skinner, D.; Ceder, G.; Persson, K. A. The Materials Project: A Materials Genome Approach to Accelerating Materials Innovation. *APL Mater.* **2013**, *1* (1), 011002.
(33) Pace, H. E.; Rogers, N. J.; Jarolimek, C.; Coleman, V. A.; Higgins, C. P.; Ranville, J. F. Determining Transport Efficiency for the Purpose of Counting and Sizing Nanoparticles via Single Particle Inductively Coupled Plasma Mass Spectrometry. *Anal. Chem.* **2011**, *83* (24), 9361−9369.
(34) Wilkin, R. T.; Rogers, D. A. Nickel Sulfide Formation at Low Temperature: Initial Precipitates, Solubility and Transformation Products. *Environ. Chem.* **2010**, *7*, 514−523.

https://doi.org/10.1021/acsearthspacechem.1c00368
ACS Earth Space Chem. XXXX, XXX, XXX−XXX

(35) Hedberg, J.; Blomberg, E.; Odnevall Wallinder, I. In the Search for Nanospecific Effects of Dissolution of Metallic Nanoparticles at Freshwater-like Conditions: A Critical Review. *Environ. Sci. Technol.* **2019**, *53* (8), 4030−4044.
(36) Zhang, C.; Hu, Z.; Deng, B. Silver Nanoparticles in Aquatic Environments: Physiochemical Behavior and Antimicrobial Mechanisms. *Water Res.* **2016**, *88*, 403−427.
(37) Narukawa, T.; Iwai, T.; Chiba, K. An ICP Index for ICP-MS Determinations-New Selection Rules for Internal Standards in ICP-MS Determinations and Carbon Enhancement Effect. *J. Anal. At. Spectrom.* **2017**, *32* (8), 1547−1553.
(38) Xiao, C. Q.; Huang, Q.; Zhang, Y.; Zhang, H. Q.; Lai, L. Binding Thermodynamics of Divalent Metal Ions to Several Biological Buffers. *Thermochim. Acta* **2020**, *691* (May), 178721.
(39) Ferreira, C. M. H.; Pinto, I. S. S.; Soares, E. V.; Soares, H. M. V. M. (Un)Suitability of the Use of pH Buffers in Biological, Biochemical and Environmental Studies and Their Interaction with Metal Ions-a Review. *RSC Adv.* **2015**, *5* (39), 30989−31003.
(40) Buchholz, A.; Laskov, C.; Haderlein, S. B. Effects of Zwitterionic Buffers on Sorption of Ferrous Iron at Goethite and Its Oxidation by CCl_4. *Environ. Sci. Technol.* **2011**, *45* (8), 3355−3360.
(41) Stemig, A. M.; Do, T. A.; Yuwono, V. M.; Arnold, W. A.; Penn, R. L. Goethite Nanoparticle Aggregation: Effects of Buffers, Metal Ions, and 4-Chloronitrobenzene Reduction. *Environ. Sci. Nano* **2014**, *1* (5), 478−487.
(42) Grady, J. K.; Chasteen, N. D.; Harris, D. C. Radicals from "Good's" Buffers. *Anal. Biochem.* **1988**, *173* (1), 111−115.
(43) Habib, A.; Tabata, M. Oxidative DNA Damage Induced by HEPES (2-[4-(2-Hydroxyethyl)-1-Piperazinyl]Ethanesulfonic Acid) Buffer in the Presence of Au(III). *J. Inorg. Biochem.* **2004**, *98* (11), 1696−1702.
(44) Lipczynska-Kochany, E.; Harms, S.; Milburn, R.; Sprah, G.; Nadarajah, N. Degradation of Carbon Tetrachloride in the Presence of Iron and Sulphur Containing Compounds. *Chemosphere* **1994**, *29* (7), 1477−1489.
(45) Zawaideh, L. L.; Zhang, T. C. The Effects of pH and Addition of an Organic Buffer (HEPES) on Nitrate Transformation in Fe0-Water Systems. *Water Sci. Technol.* **1998**, *38*, 107−115.
(46) Zhang, T. C.; Huang, Y. H. Effects of Selected Good's pH Buffers on Nitrate Reduction by Iron Powder. *J. Environ. Eng.* **2005**, *131* (3), 461−470.
(47) Morse, J. W.; Luther, G. W. Chemical Influence on Trace Metal-Sulfide Interactions in Anoxic Sediments. *Geochim. Cosmochim. Acta* **1999**, *63* (19−20), 3373−3378.
(48) Wilkin, R. T.; Beak, D. G. Uptake of Nickel by Synthetic Mackinawite. *Chem. Geol.* **2017**, *462* (April), 15−29.
(49) Hoffmann, K.; Bouchet, S.; Christl, I.; Kaegi, R.; Kretzschmar, R. Effect of NOM on Copper Sulfide Nanoparticle Growth, Stability, and Oxidative Dissolution. *Environ. Sci. Nano* **2020**, *7* (4), 1163−1178.
(50) Fulda, B.; Voegelin, A.; Ehlert, K.; Kretzschmar, R. Redox Transformation, Solid Phase Speciation and Solution Dynamics of Copper during Soil Reduction and Reoxidation as Affected by Sulfate Availability. *Geochim. Cosmochim. Acta* **2013**, *123*, 385−402.
(51) Rozan, T. F.; Lassman, M. E.; Ridge, D. P.; Luther, G. W. Evidence for Iron, Copper and Zinc Complexation as Multinuclear Sulphide Cluster in Oxic Rivers. *Nature* **2000**, *406* (6798), 879−882.
(52) Karbanee, N.; Van Hille, R. P.; Lewis, A. E. Controlled Nickel Sulfide Precipitation Using Gaseous Hydrogen Sulfide. *Ind. Eng. Chem. Res.* **2008**, *47* (5), 1596−1602.
(53) Dale, A. L.; Lowry, G. V.; Casman, E. A. Accurate and Fast Numerical Algorithms for Tracking Particle Size Distributions during Nanoparticle Aggregation and Dissolution. *Environ. Sci. Nano* **2017**, *4* (1), 89−104.
(54) Kosmulski, M. The pH Dependent Surface Charging and Points of Zero Charge. VII. Update. *Adv. Colloid Interface Sci.* **2018**, *251*, 115−138.
(55) Bebie, J.; Schoonen, M. A. A.; Fuhrmann, M.; Strongin, D. R. Surface Charge Development on Transition Metal Sulfides: An Electrokinetic Study. *Geochim. Cosmochim. Acta* **1998**, *62* (4), 633−642.
(56) Bhattacharjee, S. DLS and Zeta Potential—What They Are and What They Are Not? *J. Controlled Release* **2016**, *235*, 337−351.
(57) Wu, L.; Druschel, G.; Findlay, A.; Beard, B. L.; Johnson, C. M. Experimental Determination of Iron Isotope Fractionations among Fe_{Aq}^{2+}−FeS_{Aq}−Mackinawite at Low Temperatures: Implications for the Rock Record. *Geochim. Cosmochim. Acta* **2012**, *89*, 46−61.

https://doi.org/10.1021/acsearthspacechem.1c00368
ACS Earth Space Chem. XXXX, XXX, XXX−XXX